Spaceborne Bistatic SAR Processing Using the EETF4 Algorithm

KNUT ELDHUSET

Norwegian Defence Research Establishment (FFI)

In this letter the fourth-order Extended Exact Transfer Function (EETF4) is adapted for spaceborne bistatic SAR processing. The problems with high squint and large bistatic Doppler centroid variations are analysed and it shown that if both transmitter and receiver are highly squinted in the same direction it may be demanding to achieve perfect quality of the point targets. It is shown that if both transmitter and receiver have high squint in opposite directions with small Doppler centroid variations, then the SAR image can be processed very precisely.

I. INTRODUCTION

In the last years there has been a growing interest for processing bistatic SAR data. Most of the research has been devoted to algorithms for airborne bistatic SAR. Several novel techniques have been published and it has been concluded by several authors that the well known SAR processing algorithms such as range-Doppler (RD), chirp-scaling (CS) and the chirp Z-transform (CZT) in their original form can only be used for moderate bistatic SAR systems using a hyperbolic range equation (or azimuth phase function).

This letter focuses on spaceborne bistatic SAR processing using the fourth-order Extended Exact Transfer Function (EETF4). The EETF4 was first published in [1] for monostatic SAR processing and further analysed in [2] for ultra high resolution or high squint. In [3] it was reported that initial simulations indicated that the EETF4 may be a candidate for spaceborne bistatic SAR processing. Simultaneously, a method with some similarity to the EETF4 was extended for processing a bistatic azimuth-invariant spaceborne SAR [4]. They developed a fourth-order algorithm using the sum of two hyperbolic range functions. In [5] series reversion was applied to calculate a fourth-order two-dimensional target spectrum using the sum of two hyperbolic range functions corresponding to two linear tracks. In [6] the same authors show how this fourth-order model is used in the RD algorithm to process bistatic SAR data. In [7] they use a numerically computed transfer function which makes the azimuth phase function very accurate also for curved orbits and high squint, however, the computation of the transfer function slows down the processing speed because a two-dimensional time domain transfer function must be Fourier transformed. Another novel technique for bistatic SAR processing with linear tracks has been extensively investigated in many papers e.g. [8].

In [2] it was shown that a fourth-order azimuth phase function not using a hyperbolic function is sufficient for squint up to at least 40° for a monostatic spaceborne SAR. It was also shown that a hyperbolic azimuth phase function (which means also a series expansion of this one) is not sufficient for processing high resolution or high squint. In this letter the EETF4 with some additional features shall be analysed for bistatic SAR processing. The bistatic EETF4 takes into account curved orbits with high squint and azimuth-variant and range-variant bistatic Doppler centroids which are handled with an azimuth stretch and range stretch operation. At

Dette er en postprint-versjon / This is a postprint version.
DOI til publisert versjon / DOI to published version: 10.1109/LGRS.2008.2010781

high squint (when both transmitter and receiver are squinted in the same direction) there may also be large Doppler centroid variations in the range direction. This introduces extra challenges for the SAR processor which has been given little attention in the literature so far.

This letter begins with a short review of the fourth-order azimuth phase function extended for bistatic SAR in Section II. In Section IIIA it is shown how bistatic point target (PT) data are simulated and in IIIB the EETF4 algorithm is adapted to bistatic SAR configuration with demanding geometry. In Section IV some simulation examples are demonstrated.

II. THE AZIMUTH PHASE FUNCTION FOR SPACEBORNE BISTATIC SAR GEOMETRY

A. The bistatic range motion

The bistatic range motion of the two satellites relative to the rotating earth can be expanded up to fourth order in the same way as in [2]. Let $\vec{R}_{S,n}(t_a)$ be the position vector of either the transmitter ($n=1$) or the receiver ($n=2$) and $\vec{R}_T(t_a)$ the position vector of the target on the earth's surface, then $\vec{R}_n(t_a)=\vec{R}_{S,n}(t_a)-\vec{R}_T(t_a)$ is the relative position vector as a function of azimuth time (slow time) t_a of either the transmitter or the receiver relative to the rotating earth. We have

$$R_n(t_a)=\sqrt{\left|\vec{R}_n(t_a)\right|^2}=R_n\left(1+\frac{1}{2}x_n-\frac{1}{8}{x_n}^2+\frac{1}{16}{x_n}^3-\frac{5}{128}{x_n}^4\right) \tag{1}$$

where R_n is the range at $t_a=0$ for the transmitter ($n=1$) or for the receiver ($n=2$) and

$$x_n=a_nt_a+b_nt_a^2+c_nt_a^3+d_nt_a^4 \tag{2}$$

It was shown in [1] without the index n that

$$a_n=\frac{2\vec{V}_n\cdot\vec{R}_n}{{R_n}^2} \tag{3}$$

$$b_n=\frac{\vec{R}_n\cdot\vec{A}_n+\vec{V}_n\cdot\vec{V}_n}{{R_n}^2} \tag{4}$$

$$c_n=\frac{\vec{A}_n\cdot\vec{V}_n+\frac{1}{3}\vec{R}_n\cdot\vec{B}_n}{{R_n}^2} \tag{5}$$

$$d_n=\frac{\frac{1}{3}\vec{V}_n\cdot\vec{B}_n+\frac{1}{12}\vec{R}_n\cdot\vec{C}_n+\frac{1}{4}\vec{A}_n\cdot\vec{A}_n}{{R_n}^2} \tag{6}$$

DOI til publisert versjon / DOI to published version: 10.1109/LGRS.2008.2010781

where $\vec{V}_n$, $\vec{A}_n$, $\vec{B}_n$, $\vec{C}_n$ are the velocity, acceleration, rate of acceleration and the second derivate of the acceleration of the transmitter ($n=1$) or the receiver ($n=2$) relative to the target at $t_a = 0$. The bistatic angle is defined as the angle between the vectors $\vec{R}_1$ and $\vec{R}_2$, and bistatic distance between the transmitter and receiver is defined as $\left|\vec{R}_1 - \vec{R}_2\right|$. The bistatic range is the mean of the total distance from the transmitter to the target and from the target to the receiver

$$R(t_a) = \frac{R_1(t_a) + R_2(t_a)}{2} \tag{7}$$

and the bistatic azimuth phase function is defined by

$$\Phi(t_a) = \frac{4\pi R(t_a)}{\lambda} \tag{8}$$

where λ is the radar wavelength. For a monostatic SAR the bistatic range will be equivalent with the slant range. The azimuth Doppler frequency for a satellite SAR up to third order is defined in the bistatic case as in the monostatic case

$$f(t_a) = \frac{1}{2\pi}\frac{d\Phi(t_a)}{dt_a} \tag{9}$$

$$f(t_a) \cong f_1 + f_2 t_a + f_3 t_a^2 + f_4 t_a^3 \tag{10}$$

We use (7), (8) and (9) and see that the n'th bistatic Doppler parameter f_n can be expressed by half the sum of the monostatic Doppler parameters of the transmitter and receiver

$$f_n = \frac{f_{1,n} + f_{2,n}}{2} \tag{11}$$

where $f_{1,n}$ is the n'th monostatic Doppler parameter of the transmitter and $f_{2,n}$ is the n'th monostatic Doppler parameter of the receiver. The monostatic Doppler parameters can be estimated as in [1] for the receiver and the transmitter separately.The bistatic Doppler parameters are functions of bistatic range R

$$f_1 = f_1(R),\ f_2 = f_2(R),\ f_3 = f_3(R),\ f_4 = f_4(R) \tag{12}$$

where $R = R(0)$. The two first parameters in (12) are the bistatic Doppler centroid and the bistatic azimuth Doppler frequency rate, respectively.

III. SIMULATION OF BISTATIC SAR RAW DATA

A. Time domain simulation of raw data of point targets

Dette er en postprint-versjon / This is a postprint version.
DOI til publisert versjon / DOI to published version: 10.1109/LGRS.2008.2010781

We use a Kepler orbit as a model of the track of the SAR platform and the time domain point target response can be written

$$h_{Kepler}(t_r, t_a) = \exp\left(j\left(\frac{4\pi}{\lambda} R_{Kepler}(t_a) + \left(\Phi_r\left(t_r - \frac{2R_{Kepler}(t_a)}{c} \right) \right) \right) \right) \tag{13}$$

where $\Phi_r\left(t_r - \frac{2R_{Kepler}(t_a)}{c} \right)$ is the range phase function which also takes into account the bistatic range $R_{Kepler}(t_a)$. The bistatic range variation in (13) is exact assuming a Kepler orbit and is calculated numerically. c is the speed of light and t_r is range time (fast time). We have the bistatic range variation modelled as half the sum of the relative distance from the target to the transmitter and the receiver

$$R_{Kepler}\left(t_a\right) = \frac{R_{1,Kepler}\left(t_a\right) + R_{2,Kepler}\left(t_a\right)}{2} \tag{14}$$

The bistatic range variation in (1)-(7) is a fourth-order model of $R_{Kepler}(t_a)$ and is the basis for the bistatic EETF4 described in IIIB. We can simulate bistatic extended raw data in an approximate way using the inverse-EETF4 described in [9] (not demonstrated in this letter). Relatively small blocks are then required to simulate the raw data sufficiently exact to take into account range-variant or azimuth-variant Doppler centroid.

B. The bistatic EETF4

The flow diagram of the bistatic EETF4 algorithm is shown in Fig. 1 and the expressions for the 2D ETF4, $H^*_{ETF4}\left(\omega_r, \omega_a; R_m\right)$, and the phase corrections, $\Delta\Phi_{EETF4}\left(\omega_a; R, R_m\right)$, are given in [1]. The 2D ETF4 is multiplied by the azimuth and range FFT of the raw data. We note that the main filter $H^*_{ETF4}\left(\omega_r, \omega_a; R_m\right)$ is dependent on the bistatic Doppler parameters and can be written in the same form as in [2]

$$H^*_{ETF4}\left(\omega_r, \omega_a; R_m\right) = H^*_{ETF4}\left[\omega_r, \omega_a; f_1\left(R_m\right), f_2\left(R_m\right), f_3\left(R_m\right), f_4\left(R_m\right)\right] \tag{15}$$

where R_m is the bistatic range in the center of a block and the bistatic Doppler parameters are dependent on bistatic range as indicated in (12). The phase correction $\Delta\Phi_{EETF4}\left(\omega_a; R, R_m\right)$ is dependent on the Doppler parameters in the center of the block at bistatic range R_m and on the bistatic Doppler parameters at bistatic range R and can be written

$$\begin{aligned}\Delta\Phi_{EETF4}\left(\omega_a; R, R_m\right) = \Delta\Phi_{EETF4}\big[&\omega_a; f_1\left(R\right), f_1\left(R_m\right); f_2\left(R\right), f_2\left(R_m\right); \\ &f_3\left(R\right), f_3\left(R_m\right); f_4\left(R\right), f_4\left(R_m\right)\big]\end{aligned} \tag{16}$$

Dette er en postprint-versjon / This is a postprint version.
DOI til publisert versjon / DOI to published version: 10.1109/LGRS.2008.2010781

The phase correction in (16) is applied in each azimuth line corresponding to bistatic range R before inverse azimuth FFT and after inverse range FFT. The range frequency has been ignored in (16) and the explanation can be found in [1], Section IIIC, second paragraph. The basic algorithm is the same as the monostatic algorithm and for a bistatic SAR there may be effects like those present in a monostatic SAR at high squint. The effects are large Doppler centroid variations in range and some variation in azimuth. We talk about range variance and azimuth variance and we now show how these effects are coped with. The effect of varying Doppler centroid in range is that after inverse range FFT the first range pixel in the block migrates towards the middle of the block with an amount (measured in metres)

$$\Delta r = \frac{\lambda}{2}\left| f_1\left(1, \frac{N_{az}}{2}\right) \frac{f_1\left(1, \frac{N_{az}}{2}\right) - f_1\left(N_{ra}, \frac{N_{az}}{2}\right)}{f_2\left(\frac{N_{ra}}{2}, \frac{N_{az}}{2}\right)} \right| \tag{17}$$

where $f_1\left(1, \frac{N_{az}}{2}\right)$ and $f_1\left(N_{ra}, \frac{N_{az}}{2}\right)$ are the bistatic Doppler centroids in the first and last range pixel and azimuth pixel $\frac{N_{az}}{2}$ in a block with azimuth size N_{az} and range size N_{ra}. $f_2\left(\frac{N_{ra}}{2}, \frac{N_{az}}{2}\right)$ is the bistatic azimuth Doppler rate in the middle of the block. The block is therefore contracted with a factor $\left(\Delta R_{block} - 2\Delta r\right)/\Delta R_{block}$. The pixels can be replaced to their correct position with a range stretch interpolation which is a module in Fig. 1. The range resolution is then increased with an amount $\Delta R_{block}/\left(\Delta R_{block} - 2\Delta r\right)$ where ΔR_{block} is the bistatic range extension of a block. Then neighbouring blocks can be concatenated with size N_{ra}. In Section IV we explain (17) by using Fig. 3. In the same way we have that a block has been reduced in size in azimuth to (measured in pixels)

$$N_{az}^{'} = N_{az} - \left| \frac{\left(f_1\left(\frac{N_{ra}}{2}, 1\right) - f_1\left(\frac{N_{ra}}{2}, N_{az}\right)\right)}{f_2\left(\frac{N_{ra}}{2}, \frac{N_{az}}{2}\right)} PRF \right| \tag{18}$$

where $f_1\left(\frac{N_{ra}}{2}, 1\right)$ and $f_1\left(\frac{N_{ra}}{2}, N_{az}\right)$ are the bistatic Doppler centroids at the start and at the end of the block in azimuth in the middle of the block in range. An azimuth stretch is performed such that the block gets the size N_{az} and can be concatenated in azimuth. If the orbit of the transmitter and the receiver are the same in (14) we can also use the bistatic EETF4 for processing monostatic data.

Dette er en postprint-versjon / This is a postprint version.
DOI til publisert versjon / DOI to published version: 10.1109/LGRS.2008.2010781

IV. SIMULATION EXAMPLES

We simulate raw data for two point targets using (13). Table 1 shows the SAR parameters for the transmitter and receiver. Table 2 shows the Kepler elements of the transmitter (Tx) and receiver (Rx) for two different bistatic SAR configurations which we refer to as C1 and C2. The difference of the two cases is the mean anomalies of the transmitters. For both cases the the Kepler elements are given for the receiver in the column under Rx (C1 & C2) and for the transmitter in the two columns under Tx (C1) and Tx (C2). Tables 3 and 4 show the bistatic Doppler parameters in the two cases. We see that in the first case there is a very large bistatic Doppler centroid which changes from -182972.3 Hz to -183108.0 Hz (135.7 Hz) from range pixel 51 to range pixel 600. In the second case the bistatic Doppler centroid changes from -11.1 Hz to 15.8 Hz (26.9 Hz). The geometric difference of C1 and C2 is that for C1 both the transmitter and receiver are squinted backward and for C2 the transmitter is squinted backward and the receiver forward. The yaw angle of the transmitter is -40° in both cases. The bistatic angle is 6.8° and the bistatic distance is 78369 m for C1. For C2 the bistatic distance is 421879 m and the bistatic angle is 40.9°. For configuration C2 we used the technique described in [6] where the vector sum of the direction vectors from the target to the transmitter and the receiver is projected onto the earth's surface. As in [6] this yields small variations in the bistatic Doppler centroid over a block in range direction. Fig. 2 shows the raw data of two point targets at range pixel 51 and range pixel 600. The length of the raw data of the targets in azimuth is 10000 pixels. In Fig. 3 is a closer look in the frame shown in Fig. 2. We can see that the Doppler centroids of the two point targets have different azimuth locations marked with 'A' and 'B'. If the two PTs had the same Doppler centroid, their Doppler centroids would have the same azimuth location and PT 1 would have its Doppler centroid at location 'C' . The azimuth distance between the Doppler centroids can be calculated with $PRF \cdot |\Delta f_1| / |f_2|$ which yields $6000 \cdot 135.7 / 4814.5 = 169$ pixels.

We can understand the migration of pixels in range before the range stretch operation by looking at Fig. 3. The Doppler centroid used in the main filter is the Doppler centroid in the middle of the block where PT2 is located. There will be a time difference from 'C' to 'B', $\Delta t_{az} = \Delta f_1 / |f_2|$, corresponding to the difference of the Doppler centroid of PT1 and the Doppler centroid of PT2, Δf_1. This time difference makes PT1 migrate a distance $\Delta r = \frac{\lambda}{2} |f_1| \Delta t_{az}$ (linear range migration in a SAR processor) in range which explains the expression in (17). We see that the migration increases with increasing Doppler centroid (increasing squint), which means that we will observe an increasing range resolution loss with increasing squint when the range stretch operation is performed.

If we now use the EETF4 algorithm for C1 without the stretch operations we get the impulse responses shown in Fig. 4. The size of the block in range is 1200 pixels. The quality parameters are estimated and given in Table 5. The erronoeus azimuth and range position is 122 pixels in azimuth and 276 pixels in range for PT1 (51,51) which is near the edge of the block. In Fig. 5 are shown the point targets using range and azimuth stretch operations in the flow diagram in Fig. 1. The PT1 (51,51) have now its correct position within one pixel both in azimuth and range as is shown in Table 6. The theoretical range resolution in range can be calculated from Table 1 and is 370 MHz/300 MHz=1.23 pixels. The range pixel spacing is 0.41 m. The theoretical

Dette er en postprint-versjon / This is a postprint version.
DOI til publisert versjon / DOI to published version: 10.1109/LGRS.2008.2010781

azimuth resolution for C1 is 6000/(4812*0.85)=1.47 pixels and for C2 it is 6000/(5122*0.85)=1.38 pixels. For C2 the azimuth pixel spacing is 1.16 m. From Table 5 we see that the point in the center of the block has range resolution 1.20 and azimuth resolution 1.49, which is very close to the theoretical values. The range resolution for PT1 (51,51) is 1.33 and azimuth resolution is 1.57, which is 8.1 % and 6.8 % broadening, respectively. Table 6 shows the point targets when range and azimuth stretch are performed. The range stretch operation causes a considerable broadening in range resolution. From Table 6 we see that the broadening in range resolution is about 54 %. The peak amplitude of PT1 (51,51) is 15323 compared to 17528 of PT2 (51,600) which is a loss of 1.16 dB and the ISLR degrades 2.6 dB. If the size of a block is 300 pixels instead of 1200 pixels, the loss in amplitude is 0.1 dB and the ISLR degrades 0.3 dB. This shows that quality requirements will put limit on the block size in range when the Doppler centroid variation is large.

Fig. 6 shows the compression of the point targets using the Doppler parameters in Table 4 for the C2 configuration. The quality parameters for PT1 (51,51) and PT2 (51,600) are given in Table 7. The quality parameters are now quite close to theory which is due to the small variation of the bistatic Doppler parameters over the block. Using block size 4800 with a point target at (51,51) and (51,2400) also yields very good quality. The quality parameters are given in Table 8. We see that the quality is almost as good as with block size 1200 pixels. There is a small loss in peak amplitude of 0.06 dB. This shows that the EETF4 algorithm is very robust for very large block size when the Doppler centroid variation is small over range.

As a last test we kept the Doppler centroid constant over range in the raw data simulation in the C1 configuration. The result is shown in Table 9. The azimuth resolution is 1.54 for PT1(51,51) and 1.51 for PT2 (51,600) which is quite close to the theoretical resolution 1.47. The range resolution is 1.32 and 1.25, respectively, which is 7.3 % broadening for PT1 (51,51) and practically equal to the theoretical value for PT2 (51,600) in the middle of the block. The loss in peak amplitude of PT1 (51,51) is about 0.6 dB compared to PT2 (51,600). This example demonstrates that it is the bistatic Doppler centroid variation at high squint which causes the range resolution broadeing in the examples shown above. To obtain the best image quality in bistatic SAR images the bistatic Doppler centroid should be as low as possible and with small variations in range or azimuth. The bistatic angle and bistatic distance can be very large because when the transmitter is squinted forward and the receiver is squinted backward approximately with the same angles, the bistatic Doppler centroid and its variation over the swath may be quite small as in configuration C2.

It can be mentioned that at the resolution processed in the examples here it was shown that the EETF4 algorithm yields significantly better point target responses than the EETF2 at $yaw = -5^{\circ}$ for a configuration similar to C1. The ISLR is around -14.2 dB for EETF2 and -16.2 dB for EETF4. The peak amplitude loss is about 0.3 dB. At $yaw = -10^{\circ}$ the ISLR is about -11.8 dB for EETF2 and -16.0 for EETF4.

V. CONCLUSIONS

The monostatic EETF4 algorithm has been adapted to process bistatic SAR data and the problem with high bistatic Doppler centroid variations has been investigated. If both transmitter and receiver are squinted in the same direction the SAR point targets can however be processed with somewhat reduced quality parameters when

Dette er en postprint-versjon / This is a postprint version.
DOI til publisert versjon / DOI to published version: 10.1109/LGRS.2008.2010781

the squint is very large (e.g. $yaw = -40^{\circ}$). If the transmitter and receiver are squinted in opposite directions with high angles the quality of the point targets is close to what can be achieved using time domain processing.

ACKNOWLEDGMENT

This work was supported by the Norwegian Defence Research Establishment (FFI).

VI. REFERENCES

[1] Eldhuset, K. (1998) A New Fourth-Order SAR Processing Algorithm for Spaceborne SAR. *IEEE Transactions on Aerospace and Electronic Systems*, **34**, 3 (July 1998), 824-835.

[2] Eldhuset, K. (2004) Ultra High Resolution Spaceborne SAR Processing. *IEEE Transactions on Aerospace and Electronic Systems*, **40**, 1 (July 2004), 370-378.

[3] Arnesen, T.N., Eldhuset, K., Weydahl, D.J. (2006) Modelling of Scattering from Point Like Targets. In Proceedings of IGARSS'06, Denver, USA , Aug. 2006.

[4] Zhong, H., Liu, X. (2006) A Fourth-Order Imaging Algorithm for Spaceborne Bistatic SAR. In Proceedings of IGARSS'06, Denver, USA , Aug. 2006.

[5] Neo, Y.L., Wong, F., Cumming, I.G. (2007) A Two-Dimensional Spectrum for Bistatic SAR Processing Using Series Reversion. *IEEE Transactions on Geoscience and Remote Sensing*, 4, 1 (January 2007), 93-96.

[6] Neo, Y.L., Wong, F., Cumming, I.G. (2008) Processing of Azimuth-Invariant Bistatic SAR Data Using the Range Doppler Algorithm. *IEEE Transactions on Geoscience and Remote Sensing*, 46, 1 (January 2008), 14-21.

[7] Bamler, R., Meyer, F., Liebhart, W. (2007) Processing of Bistatic SAR Data From Quasi-Stationary Configuration. *IEEE Transactions on Geoscience and Remote Sensing*, 45, 11 (November 2007), 3350-3358.

[8] Natroshvili, K., Loffeld, O., Nies, H., Ortiz, A.M. and Knedlik, S. (2006) Focusing of General Bistatic SAR Configuration Data With 2-D Inverse Scaled FFT. *IEEE Transactions on Geoscience and Remote Sensing*, 44, 10 (October 2006), 2718-2727.

[9] Eldhuset, K. (2005) High Resolution Spaceborne INSAR Simulation with Extended Scenes. *IEE Proceedings Radar, Sonar & Navigation*, **152**, 2 (April 2005), 53-57.

Fig. 1 The flow diagram for the bistatic EETF4

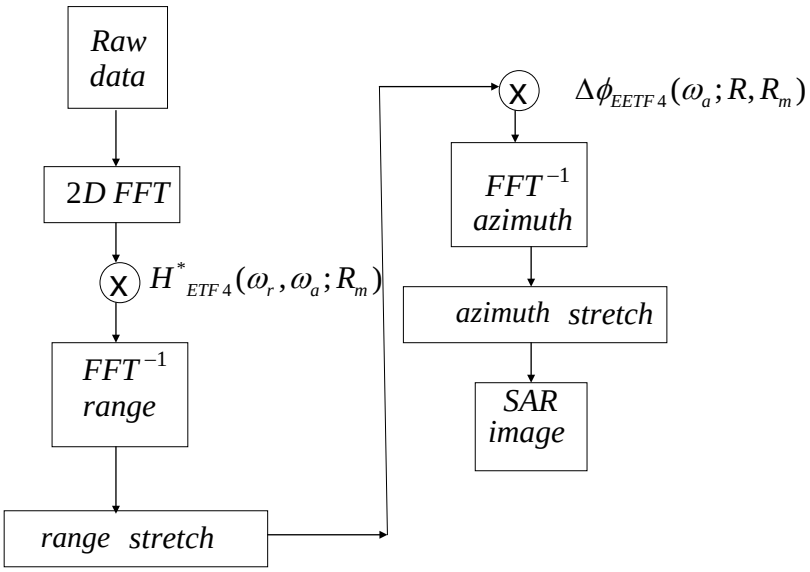

Dette er en postprint-versjon / This is a postprint version.
DOI til publisert versjon / DOI to published version: 10.1109/LGRS.2008.2010781

Fig. 2 Raw data of two point targets for configuration C1. The yaw angle of the beam is -40° . PT1 is the point target at range pixel 51 and PT2 at range pixel 600.

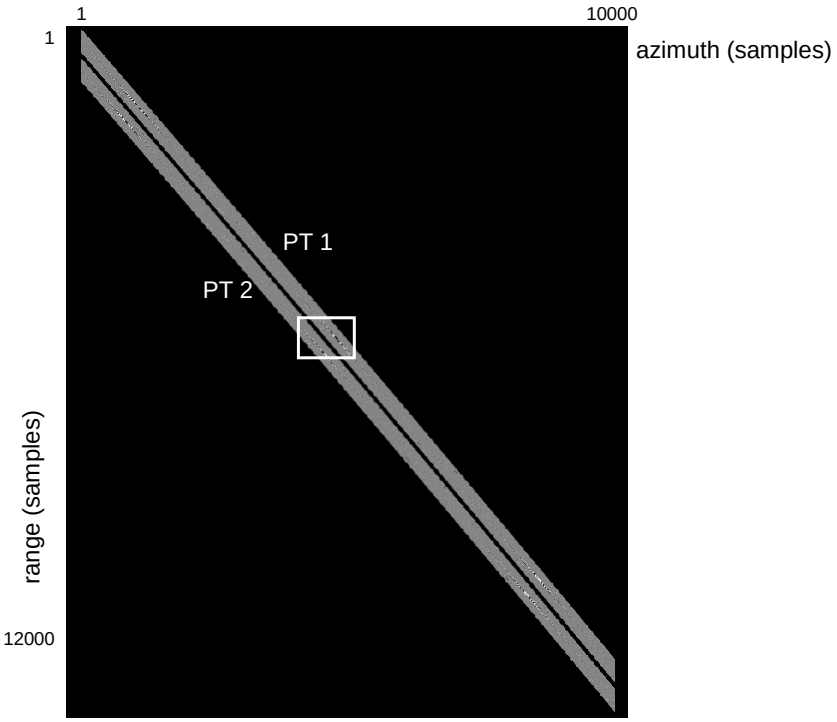

Fig. 3 Zoom of the raw data of the two point targets in the small frame in Fig. 2

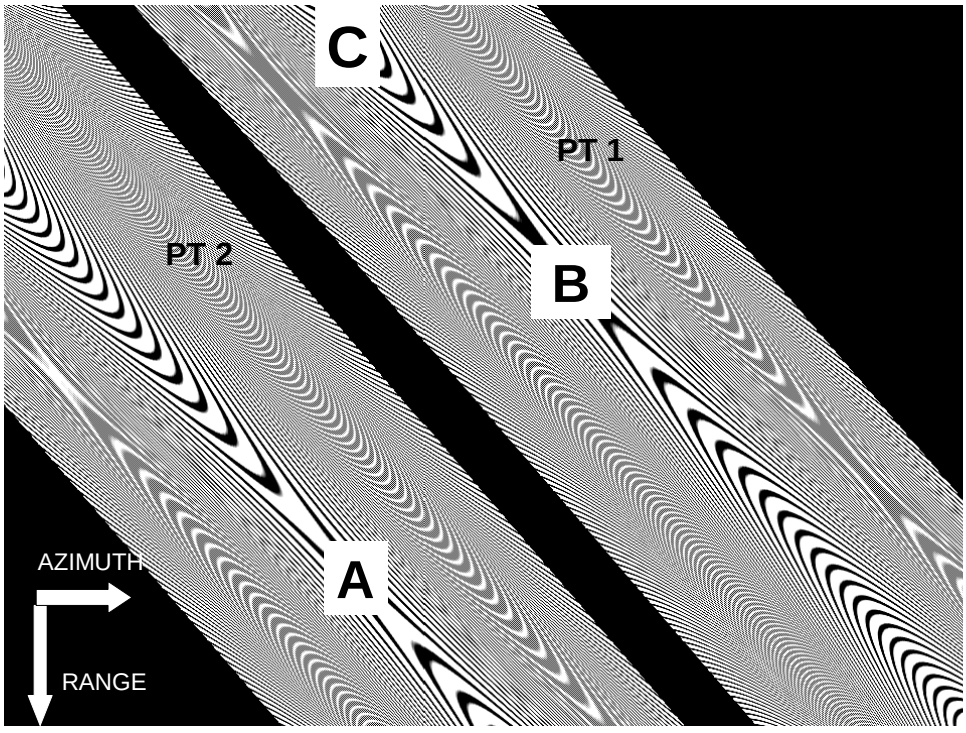

Dette er en postprint-versjon / This is a postprint version.
DOI til publisert versjon / DOI to published version: 10.1109/LGRS.2008.2010781

Fig. 4 Compressed raw data in Fig. 2 without stretching (C1)

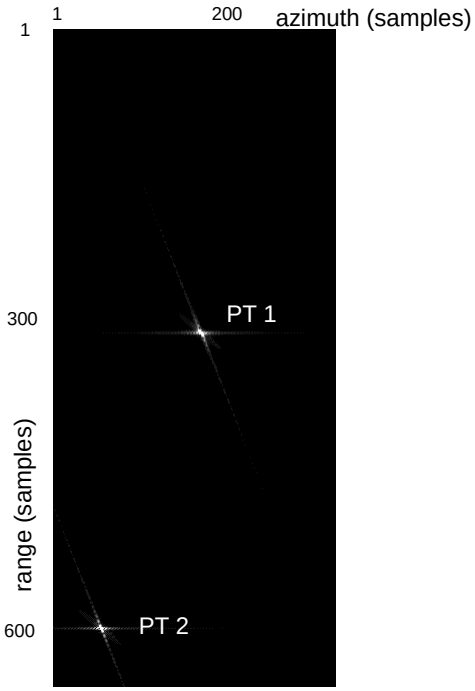

Fig. 5 Compressed raw data in Fig. 2 with stretch interpolation in azimuth and range (C1)

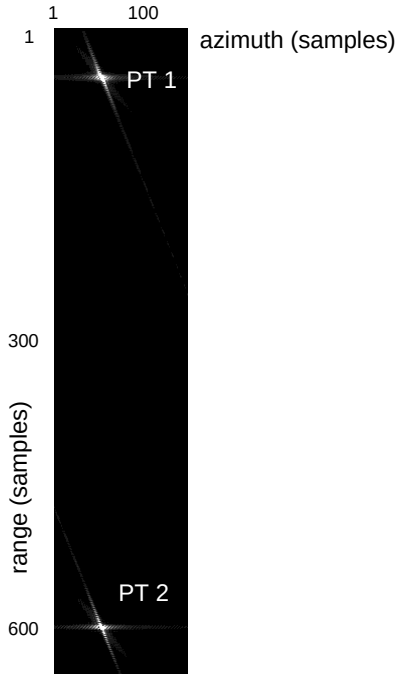

DOI til publisert versjon / DOI to published version: 10.1109/LGRS.2008.2010781

Fig. 6 Compressed raw data for the C2 configuration

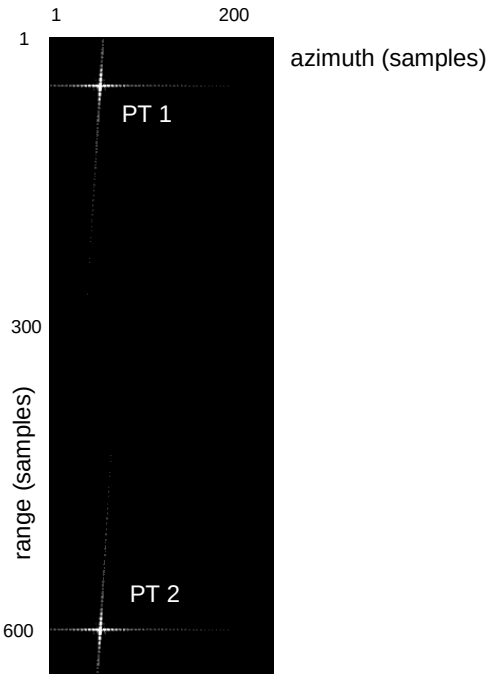

Table 1 SAR parameters used in the simulations for receiver and transmitter.

Table 2 The Kepler elements for the receiver Rx and transmitter Tx for two configurations C1 and C2.

Table 3 Bistatic Doppler parameters for C1 where $yaw = -40^{\circ}$ for X-band. Bistatic distance is 78369 m. Latitude is 55.7° deg. Bistatic angle is 6.8°

Table 4 Bistatic Doppler parameters for C2 where $yaw = -40^{\circ}$ for X-band. Bistatic distance is 421879 m. Latitude is 59.3° deg. Bistatic angle is 40.9°

Table 5 Quality parameter measurements of point targets in Fig. 4

Table 6 Quality parameter measurements of point targets in Fig. 5

Table 7 Quality parameter measurements of point targets in C2 with block size 1200 in range

Table 8 Quality parameter measurements of point targets in C2 with same Doppler parameters as in Table 7 with block size 4800 in range

Table 9 Quality parameter measurements of point targets in C1 using constant Doppler centroid over the block

DOI til publisert versjon / DOI to published version: 10.1109/LGRS.2008.2010781

TABLE 1

RF-center frequency	9.6 GHz
Range chirp bandwidth	300 MHz
Range chirp duration	1.25 μs
Sampling frequency	370 MHz
Azimuth raw PT length	1.67 s
Azimuth filter length	0.85 s

TABLE 2

	Rx (C1 & C2)	Tx (C1)	Tx (C2)
a : Semimajor axis (m)	6886008	6886008	6886008
i : Inclination (°)	98.0	98.0	98.0
e : Eccentricity	0.001	0.001	0.001
ω : Argument of perigee (°)	90.0	90.0	90.0
Ω : Ascending node (°)	0.0	0.0	0.0
M : Mean anomaly (°)	270.07	270.72	266.55

TABLE 3

$R_1(m)$	$R_2(m)$	$f_1(s^{-1})$	$f_2(s^{-2})$	$f_3(s^{-3})$	$f_4(s^{-4})$
599916	628195	-182972.3	-4814.5	33.375	0.09096
600127	628426	-183108.0	-4811.5	33.367	0.09046

TABLE 4

$R_1(m)$	$R_2(m)$	$f_1(s^{-1})$	$f_2(s^{-2})$	$f_3(s^{-3})$	$f_4(s^{-4})$
600325.0	606605.1	-11.1	-5123.3	0.34906	0.1650
600513.8	606832.3	15.8	-5121.9	0.34665	0.1673

TABLE 5

(az,ra)	Peak amplitude	ISLR (dB)	Range res (pixels)	Azimuth res (pixels)	Err pos (az,ra)
(51,51)	15438	-14.0	1.33	1.57	(122,276)
(51,600)	17822	-15.6	1.20	1.49	(2,0)

Dette er en postprint-versjon / This is a postprint version.
DOI til publisert versjon / DOI to published version: 10.1109/LGRS.2008.2010781

TABLE 6

(az,ra)	Peak amplitude	ISLR (dB)	Range res (pixels)	Azimuth res (pixels)	Err pos (az,ra)
(51,51)	15323	-13.7	1.98	1.60	(-0.8,-0.6)
(51,600)	17528	-16.3	1.88	1.49	(-0.9,-0.8)

TABLE 7

(az,ra)	Peak amplitude	ISLR (dB)	Range res (pixels)	Azimuth res (pixels)	Err pos (az,ra)
(51,51)	17501	-16.2	1.30	1.41	(0.2,-1.1)
(51,600)	17510	-16.1	1.30	1.41	(0.2,-1.1)

TABLE 8

(az,ra)	Peak amplitude	ISLR (dB)	Range res (pixels)	Azimuth res (pixels)	Err pos (az,ra)
(51,51)	17680	-16.0	1.33	1.39	(0.2,-1.1)
(51,2400)	17807	-16.2	1.30	1.38	(0.1,-1.1)

TABLE 9

(az,ra)	Peak amplitude	ISLR (dB)	Range res (pixels)	Azimuth res (pixels)	Err pos (az,ra)
(51,51)	16176	-15.4	1.32	1.54	(1.1,1.1)
(51,600)	17286	-16.1	1.25	1.51	(0.1,0.1)

DOI til publisert versjon / DOI to published version: 10.1109/LGRS.2008.2010781